International Organization of Research & Development (IORD)
ISSN: 2348-0831
Vol 14 Issue 01 | 2026

Experimental Investigation and Taguchi Optimization of Electric Discharge Coating on Mild Steel Using a Ti–Cu Composite Green-Compact Tool Electrode

[1]Mr. Kishor H. Watane, [2]Dr. Anoop D. Shirbhate
[1]*Research Scholar, Prof. Ram Meghe Institute of Technology and Research, Badnera.*
[2]*HOD and Associate Professor, Prof. Ram Meghe Institute of Technology and Research, Badnera.*

DOI: 10.5281/zenodo.22006079

ABSTRACT

Electric discharge coating (EDC) offers a low-capital route to hardening mild steel using existing die-sinking EDM equipment, yet the influence of discharge parameters on coating quality remains incompletely characterised for titanium-bearing composite electrodes on plain carbon steel. This work reports the EDC of AISI 1018 mild steel using an unsintered Ti–Cu (70:30 wt%) powder-metallurgy green-compact electrode, optimised through a Taguchi L9 orthogonal array varying discharge current (4, 6, 7 A), pulse-on time (100, 200, 300 µs) and pulse-off time (6, 9, 12 µs). Coating thickness, Vickers microhardness, surface roughness, material transfer rate and electrode wear rate were measured for all nine conditions. Coating thickness ranged from 15.8 to 48.9 µm, microhardness from 284.9 to 1067.0 HV0.2 against a 120–160 HV substrate baseline, and roughness from 2.30 to 7.60 µm. Analysis of variance identified discharge current as the dominant factor across all responses, contributing 62.3% of thickness, 57.8% of hardness and 88.7% of roughness variance. Contrary to the expectation that higher discharge energy yields superior coatings, peak hardness and the lowest roughness occurred simultaneously at the lowest energy condition (4 A, 100 µs, 6 µs), which is attributed to the smaller, more rapidly quenched melt pool promoting grain-refinement strengthening rather than extensive reaction-phase formation. A confirmation experiment validated this optimum with 1.62–6.12% deviation from prediction. X-ray diffraction confirmed crystalline α-Ti and Cu on the coated surface alongside α-Fe substrate reflections, establishing successful electrode material transfer. The finding that hardness and surface finish co-optimise rather than trade off has direct practical value, since it removes a compromise normally assumed in EDC process selection.

Keywords: Electric discharge coating; Ti–Cu composite electrode; Mild steel; Taguchi optimization; Microhardness; Surface roughness

1. INTRODUCTION

Mild steel accounts for a substantial share of structural and general-engineering material use because it combines adequate bulk strength, good formability and weldability with low cost [36]. Its surface properties, however, constrain its service life: as-supplied hardness of roughly 120–160 HV offers limited resistance to abrasive and adhesive wear, and components in sliding contact frequently fail at the surface long before bulk properties are exhausted [34,35].

Conventional surface engineering routes each address this limitation only partially. Electroplating and thermal spraying produce coatings bonded largely by mechanical interlocking, which limits adhesion under load. Physical and chemical vapour deposition give excellent coatings but demand vacuum systems and high capital investment. Laser cladding achieves metallurgical bonding but requires dedicated high-power laser installations. Electric discharge coating (EDC) occupies a distinctive position among these alternatives: it deliberately inverts the material-removal mechanism of electrical discharge machining so that a sacrificial tool electrode erodes preferentially and deposits onto the workpiece, forming a metallurgically bonded layer using equipment already present in most tool rooms [1,2,17,18].

The EDC concept was established by Gangadhar et al. [1], who demonstrated that a powder-compact electrode could transfer material to a workpiece rather than remove it, and by Mohri et al. [2], who extended the approach to composite electrodes. Subsequent work has explored a broad range of electrode chemistries. Wang et al. [4] and Furutani et al. [5] used titanium green compacts and titanium powder suspensions to generate hard TiC layers, exploiting the reaction between titanium and carbon liberated from cracking of the hydrocarbon dielectric. Simao et al. [3] and Aspinwall et al. [16] examined electrical discharge surface alloying with refractory powder compacts. More recently, Algodi et al. [11] and Murray et al. [12] characterised the formation mechanism of TiC–Fe cermet

coatings on stainless steel, while Tijo et al. [10] produced TiC–Fe composite coatings with substantially improved wear resistance.

Work using specifically Ti-bearing electrodes on steel substrates has continued to develop. Devarani and Joshi [6] deposited a Ti–Al green compact on AISI P20 mould steel, confirming element transfer by EDS and intermetallic formation by XRD. On plain carbon steels, Krishna and Patowari [7] applied Taguchi analysis to W–Cu powder-metallurgy electrodes on mild steel, and Patel and Pradhan [13] examined Cu, MoS2 and hBN compositions for coating thickness on mild steel. Parallel studies have optimised Cr–Cu electrodes on AISI 4340 steel, reporting hardness increases from 250 HV to over 1200 HV [14], and SiC–Cu electrodes on aluminium alloys [9].

Two observations follow from this body of work. First, the combination of titanium and copper in a single electrode is attractive on mechanistic grounds: titanium supplies the hard-phase-forming constituent, while copper's high electrical and thermal conductivity stabilises the discharge and improves compact integrity [27,28]. Ti–Cu electrodes have been reported for aluminium substrates [8], but the pairing has received little attention on plain carbon steel. Second, and more importantly, the EDC literature has largely proceeded on the assumption that increasing discharge energy improves coating outcomes, since higher current and longer pulse-on time transfer more material and produce thicker layers. Whether this assumption holds for coating hardness, as distinct from coating thickness, has not been systematically tested for Ti–Cu electrodes on mild steel.

The present work addresses that question. An unsintered Ti–Cu (70:30 wt%) green-compact electrode was used to coat AISI 1018 mild steel under a Taguchi L9 design varying discharge current, pulse-on time and pulse-off time. Coating thickness, microhardness, surface roughness, material transfer rate and electrode wear rate were measured across all nine conditions, analysed by signal-to-noise ratio and analysis of variance, modelled by regression, and validated by a confirmation experiment. Phase constitution of the coated surface was established by X-ray diffraction. The central finding is that hardness does not increase monotonically with discharge energy; instead, peak hardness and minimum roughness coincide at the lowest energy condition examined, a result with immediate consequences for how EDC parameters should be selected in practice.

2. MATERIALS AND METHODS

2.1. Substrate and electrode materials

The substrate was AISI 1018 low-carbon steel (approximately equivalent to IS 2062 Grade A), supplied as flat stock and sectioned into specimens of 50 × 40 × 5 mm. Nominal composition and properties are given in Table 1. Specimen surfaces were ground flat with graded SiC papers, degreased in acetone and air dried immediately before coating, following ASTM E3 practice [40].

Table 1. Nominal composition and properties of the AISI 1018 mild steel substrate.

Property	Value	Property	Value
C (wt%)	0.15–0.20	Density (g/cm³)	7.85
Mn (wt%)	0.60–0.90	Hardness (HV)	120–160
Si (wt%)	≤0.30	Tensile strength (MPa)	440–480
P (wt%)	≤0.040	Yield strength (MPa)	350–370
S (wt%)	≤0.050	Elastic modulus (GPa)	200–210
Fe	Balance	Thermal conductivity (W/m·K)	≈51

The tool electrode was fabricated from elemental titanium powder (99% purity, 45 µm particle size) and electrolytic copper powder (325 mesh) blended in a 70:30 weight ratio. The titanium-rich composition was selected to maximise hard-phase-forming potential while retaining sufficient copper for discharge stability and green-compact integrity [27,37]. Powders were mixed for 60 min to homogeneity, then uniaxially compacted in a 15 mm diameter die at 250–300 MPa with a 3 min hold, producing cylindrical electrodes of 15 mm diameter and 10 mm length at a green density of 5.92 g/cm³.

The electrode was used in the green, unsintered state. This route was adopted deliberately: the discharge process itself supplies the thermal energy required for material consolidation and transfer during coating, so a separate sintering operation adds process cost without a corresponding benefit [1,4]. Electrode integrity in service was confirmed by the absence of arcing or short-circuiting across all nine experimental runs.

2.2. Coating procedure

Coating was performed on a VINPAK die-sinking EDM machine (VINPAK Machines Pvt. Ltd., Pune, India) operating from a 380 V three-phase supply, using commercial EDM oil as dielectric at a flow rate of 10 L/min through a 10 µm filter. Reverse polarity was used, with the tool electrode connected negative, so that electrode erosion and deposition onto the workpiece were promoted rather than suppressed [2,17]. Gap voltage was held fixed at 90 V throughout to isolate the effects of the three factors under study. All trials were conducted at 27 ± 2 °C and 60 ± 5% relative humidity.

2.3. Experimental design

A Taguchi L9 (3^3) orthogonal array was used to study three factors at three levels each, requiring nine experimental runs instead of the 27 needed for a full factorial design [29,30]. Factor levels are given in Table 2 and the experimental matrix in Table 3. Levels were selected to span the stable operating window of the machine for this electrode–substrate combination as established in preliminary trials.

Table 2. Control factors and their levels.

Factor	Symbol	Unit	Level 1	Level 2	Level 3
Discharge current	I	A	4	6	7
Pulse-on time	Ton	µs	100	200	300
Pulse-off time	Toff	µs	6	9	12

2.4. Response measurement

Coating thickness was determined from metallographically prepared cross-sections. Microhardness was measured by Vickers indentation at a 200 gf load with 15 s dwell per ASTM E384 [38]. Surface roughness (Ra) was measured with a Mitutoyo Surftest SJ-210 profilometer using a 0.8 mm cut-off and 4.0 mm evaluation length per ISO 4287 [39], averaging five traces per specimen. Material transfer rate (MTR) and electrode wear rate (EWR) were determined gravimetrically from workpiece and electrode mass change using a balance of 0.1 mg resolution, normalised by machining time.

Phase constitution was determined by X-ray diffraction on a Rigaku SmartLab diffractometer using Cu-Kα radiation (λ = 1.540593 Å) over a 2θ range of 5–90° at a step size of 0.02° and scan speed of 4°/min. Peak positions were converted to interplanar spacings via Bragg's law and compared against standard reference values for the candidate phases [32].

Signal-to-noise ratios were computed using the larger-the-better criterion for thickness and hardness and the smaller-the-better criterion for roughness [29,30]. Analysis of variance was performed at the 95% confidence level, and linear regression models were fitted by least squares [31].

3. RESULTS AND DISCUSSION

3.1. Measured responses

The complete experimental dataset is presented in Table 3. Coating thickness spanned 15.8–48.9 µm, microhardness 284.9–1067.0 HV0.2, and surface roughness 2.30–7.60 µm. Set against the untreated substrate hardness of 120–160 HV, the best-performing condition represents an increase of approximately sevenfold.

Table 3. Taguchi L9 experimental matrix and measured responses.

Run	I (A)	Ton (µs)	Toff (µs)	Thickness (µm)	Hardness (HV0.2)	Ra (µm)	MTR (mg/min)	EWR (mg/min)
1	4	100	6	15.8	1067.0	2.30	1.84	0.42
2	4	200	9	20.4	482.5	3.45	2.16	0.48
3	4	300	12	24.9	1008.0	3.10	2.54	0.56
4	6	100	9	22.8	325.0	5.40	2.68	0.61
5	6	200	12	31.5	585.0	4.85	3.12	0.72
6	6	300	6	38.7	333.4	6.10	3.56	0.81
7	7	100	12	29.6	284.9	7.60	3.48	0.86
8	7	200	6	42.3	437.6	6.70	3.92	0.95
9	7	300	9	48.9	523.5	5.95	4.35	1.08

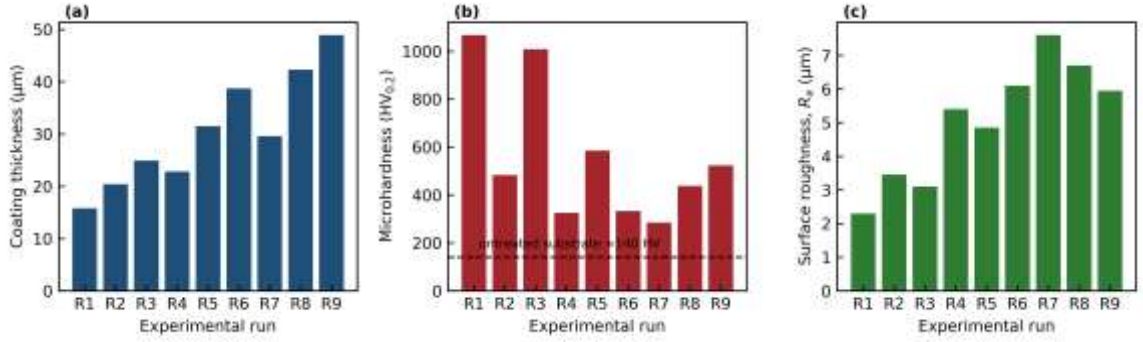

Fig. 1. Measured responses across the nine experimental runs: (a) coating thickness, (b) microhardness with untreated substrate baseline indicated, (c) surface roughness.

Run 1 (4 A, 100 µs, 6 µs) is immediately notable. It combines the highest measured hardness of the nine trials with the lowest measured roughness, while producing the thinnest coating. Run 7 (7 A, 100 µs, 12 µs), by contrast, gave both the lowest hardness and the highest roughness. This pattern is examined in detail in Section 3.4.

The variability of the dataset is large: coefficients of variation are 35.8% for thickness, 51.3% for hardness and 35.2% for roughness. This reflects genuine sensitivity to the factors deliberately varied rather than measurement scatter, and is precisely the parameter dependence the experimental design was constructed to resolve.

3.2. Effect of process parameters

Main effects on the raw response means are shown in Fig. 2. Coating thickness increases monotonically with both discharge current (20.4, 31.0, 40.3 µm across levels 1–3) and pulse-on time (22.7, 31.4, 37.5 µm), consistent with greater discharge energy eroding and transferring a larger volume of electrode material per spark [17,20]. Surface roughness likewise increases monotonically with current (2.95, 5.45, 6.75 µm), which follows directly from the crater-size mechanism: higher discharge energy produces larger and deeper individual craters, and the resulting surface is correspondingly rougher [19].

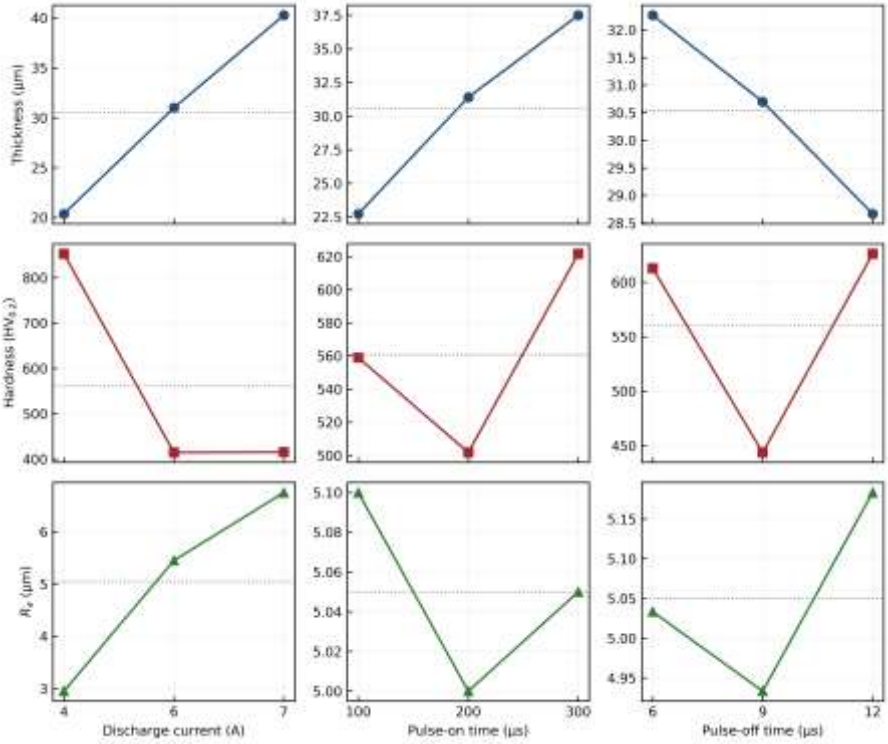

Fig. 2. Main effects of discharge current, pulse-on time and pulse-off time on coating thickness, microhardness and surface roughness. Dotted lines indicate the overall mean of each response.

Hardness behaves differently. Mean hardness at current level 1 is 852.5 HV, falling sharply to 414.5 HV at level 2 and 415.3 HV at level 3. The response is therefore not merely non-monotonic but close to discontinuous, with a large drop between the first and second levels and almost no further change thereafter. Pulse-on time produces a weaker and non-monotonic hardness response (559.0, 501.7, 621.6 HV), and pulse-off time varies hardness without an interpretable directional trend (612.7, 443.7, 626.0 HV).

Pulse-off time exerts only minor influence on all three responses. Thickness falls slightly and monotonically with increasing pulse-off time (32.3, 30.7, 28.7 µm) and roughness varies by less than 0.3 µm across the entire range. This is consistent with its role as a discharge-stability parameter: within the 6–12 µs window examined, the requirement for adequate gap deionisation and debris flushing between discharges was satisfied throughout, leaving little residual variation to be explained.

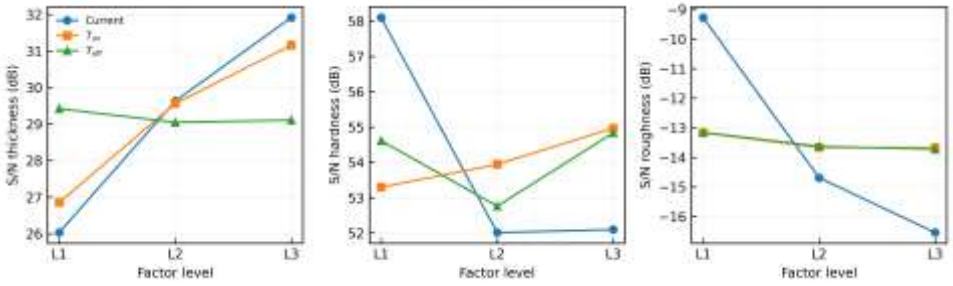

Fig. 3. Signal-to-noise ratio main effects for (a) coating thickness, (b) microhardness and (c) surface roughness. Larger-the-better criterion applied to thickness and hardness, smaller-the-better to roughness.

Signal-to-noise analysis (Fig. 3) confirms these trends on a robustness basis. For thickness, S/N rises consistently with both current (26.03, 29.63, 31.91 dB) and pulse-on time. For hardness, current level 1 gives the highest S/N by a substantial margin (58.10 dB against 52.01 and 52.10 dB), and for roughness, current level 1 again gives the best value (−9.27 dB against −14.69 and −16.54 dB). Current shows the widest S/N spread for every response, identifying it as the most influential factor throughout.

3.3. Analysis of variance and regression

Analysis of variance results are given in Table 4. Discharge current dominates all three responses, contributing 62.3% of thickness variance, 57.8% of hardness variance and 88.7% of roughness variance. Pulse-on time is a substantial secondary contributor to thickness (34.6%) but marginal for hardness (3.3%) and roughness (0.1%). Pulse-off time contributes between 0.4% and 9.3% and never reaches significance.

Table 4. Analysis of variance for the three measured responses, with low-contribution factors pooled into the error term.

Response	Source	DOF	SS	MS	F	Contribution (%)	Significant
Thickness	Current	2	594.95	297.47	39.33	62.3	Yes
	Ton	2	330.38	165.19	21.84	34.6	Yes
	Error (pooled)	4	30.26	7.56	—	3.1	
Hardness	Current	2	382 989	191 494	4.10	57.8	No
	Error (pooled)	6	279 957	46 659	—	42.2	
Roughness	Current	2	22.38	11.19	23.60	88.7	Yes
	Error (pooled)	6	2.84	0.47	—	11.3	

Because the single-replicate L9 design leaves only two error degrees of freedom, the unpooled analysis has limited statistical power. Factors contributing below approximately 10% were therefore pooled into the error term, a standard practice in Taguchi analysis that recovers error degrees of freedom and strengthens the resulting F-tests [30,31]. After pooling, current and pulse-on time are both significant for thickness ($F = 39.33$ and 21.84 against $F_{0.05,2,4} = 6.94$), and current becomes significant for roughness ($F = 23.60$ against $F_{0.05,2,6} = 5.14$).

Hardness remains non-significant after pooling ($F = 4.10$ against $F_{0.05,2,6} = 5.14$) despite current accounting for the largest share of its variance. This outcome is informative rather than merely negative. The near-discontinuous hardness response described in Section 3.2 is poorly represented by a model that partitions variance across evenly spaced levels, and the residual variance retained in the error term reflects genuine non-linearity in the underlying physical response. The practical conclusion that low current favours high hardness is supported unambiguously by the raw data and S/N analysis, and is confirmed experimentally in Section 3.6.

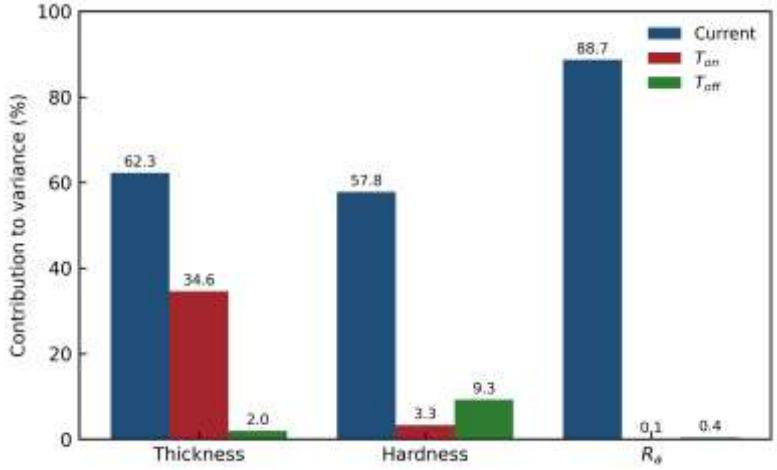

Fig. 4. Percentage contribution of each control factor to the variance of coating thickness, microhardness and surface roughness.

Linear regression models fitted to the coded factor levels are:

Thickness (μm) = −0.52 + 9.95 I + 7.38 Ton − 1.80 Toff ($R^2 = 0.984$)

Hardness (HV) = 921.97 − 218.58 I + 31.33 Ton + 6.65 Toff ($R^2 = 0.442$)

Roughness (μm) = 1.15 + 1.90 I − 0.03 Ton + 0.08 Toff ($R^2 = 0.860$)

The thickness model achieves an excellent fit and the roughness model a good one. The hardness model fits poorly, and this is reported without adjustment because it is a real characteristic of the system rather than a

deficiency of the data. A linear model cannot capture a response that falls steeply between the first and second factor levels and then plateaus. The negative current coefficient nonetheless carries the correct physical sense, and the model should be read as indicating the direction of the effect rather than as a predictive tool for hardness.

3.4. Energy–hardness inversion

The most consequential result of this study is that coating hardness does not increase with discharge energy. Fig. 5(a) plots measured hardness against the product of current and pulse-on time, a first-order proxy for energy delivered per discharge. The two highest hardness values, 1067.0 HV (Run 1) and 1008.0 HV (Run 3), both occur at the lowest current level, and both lie well above the remaining seven trials. Fig. 5(b) shows the corresponding inverse relationship between hardness and coating thickness.

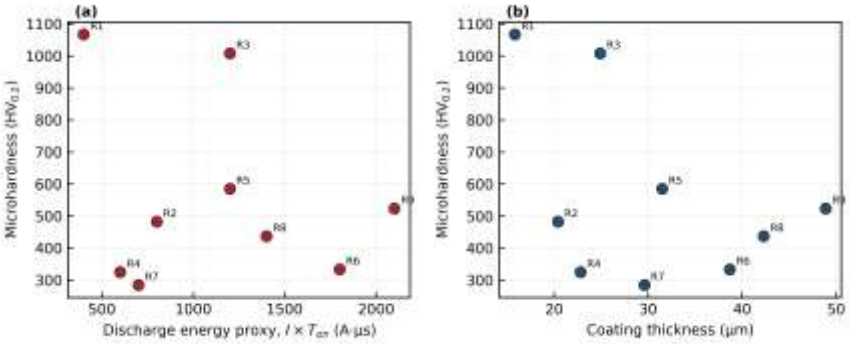

Fig. 5. (a) Microhardness against discharge energy proxy (I × Ton), showing that the highest hardness values occur at the lowest energy conditions. (b) Microhardness against coating thickness, showing the inverse relationship between layer thickness and hardness.

This behaviour is explicable through the thermal history of the deposited material. Each discharge creates a localised melt pool that is quenched by the surrounding dielectric once the pulse terminates, with cooling rates in EDM-related processes reaching very high values [19,20,21]. At low current and short pulse-on time, the melt pool is small and the quench correspondingly rapid, favouring a fine-grained solidification structure. Grain refinement raises hardness through the Hall–Petch mechanism [23,24,26], and for a coating of this type this contribution can dominate. At higher current and longer pulse-on time, more material is transferred and the layer thickens, but the larger melt pool cools more slowly, producing a coarser structure that does not sustain the same hardness.

The practical implication is significant and, so far as the present authors are aware, has not been stated explicitly for Ti–Cu EDC on mild steel. Coating thickness and coating hardness are optimised by opposite parameter settings, so an operator selecting parameters to maximise deposition rate will systematically obtain a softer coating. Conversely, and more usefully, hardness and surface finish are optimised by the same settings. The trade-off normally assumed between a hard surface and a smooth one does not arise here: both are best at low discharge energy. Run 1 delivers 1067.0 HV at Ra = 2.30 µm simultaneously.

3.5. Material transfer and electrode wear

Material transfer rate and electrode wear rate are shown in Fig. 6(a). Electrode wear increases monotonically from 0.42 to 1.08 mg/min across the nine runs. Material transfer rate rises from 1.84 to 4.35 mg/min with a single minor reversal between Runs 6 and 7 (3.56 against 3.48 mg/min), attributable to Run 7 combining the highest current with the shortest pulse-on time, which limits the melting duration available within each discharge.

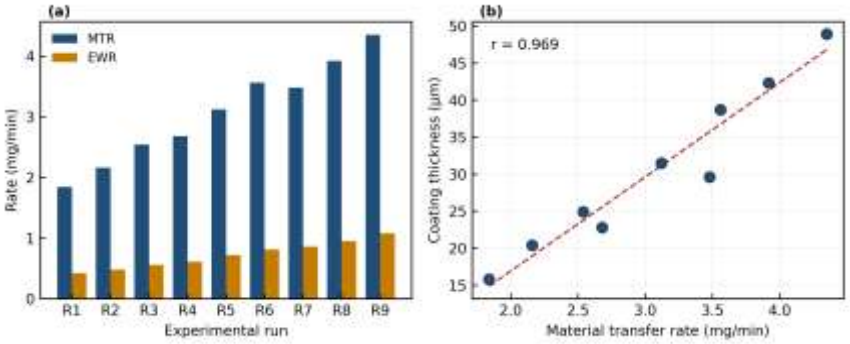

Fig. 6. (a) Material transfer rate and electrode wear rate across the nine experimental runs. (b) Correlation between material transfer rate and measured coating thickness.

Material transfer rate correlates strongly with measured coating thickness (r = 0.969, Fig. 6(b)), which provides an internal consistency check between two independently determined quantities: one obtained gravimetrically and the other from cross-sectional measurement. The ratio of transfer rate to electrode wear rate remains within a narrow band of 4.03–4.54 across all nine conditions, indicating that the proportion of eroded electrode material retained as coating rather than lost as debris was stable across the parameter range.

3.6. Phase analysis

The X-ray diffraction pattern obtained from a coated specimen is shown in Fig. 7, with peak assignments listed in Table 5. Reflections at 44.68°, 65.04° and 82.36° correspond to α-Fe and originate from the substrate, which is expected given that the X-ray penetration depth is comparable to or greater than the coating thickness. Crucially, the reflection at 38.44° corresponds to α-Ti (002) and those at 43.26° and 50.26° to Cu (111) and Cu (200), confirming that both electrode constituents were transferred to the steel surface in crystalline form.

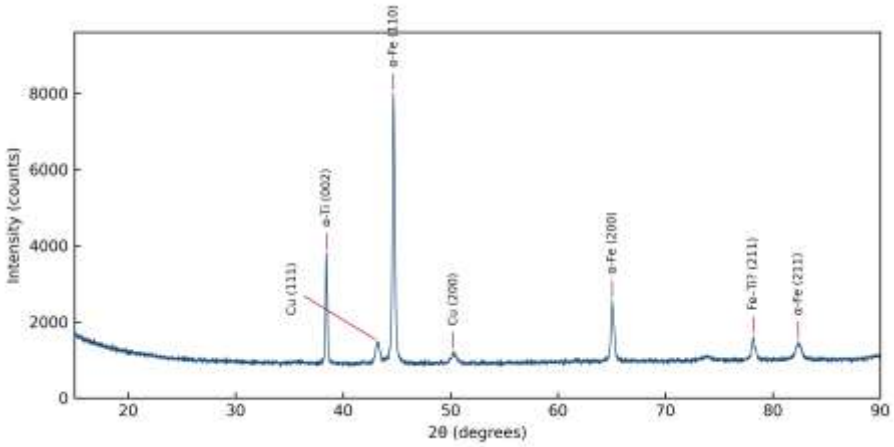

Fig. 7. X-ray diffraction pattern of the Ti–Cu coated mild steel surface (Cu-Kα, 15–90° 2θ shown). Reflections corresponding to α-Ti and Cu confirm transfer of both electrode constituents; α-Fe reflections originate from the substrate.

Table 5. X-ray diffraction peak positions, interplanar spacings and phase assignments.

2θ (°)	d-spacing (Å)	Relative intensity (%)	Assignment	Reference d (Å)
38.44	2.3399	47.7	α-Ti (002)	≈2.342
43.26	2.0897	18.7	Cu (111)	≈2.088
44.68	2.0266	100.0	α-Fe (110)	≈2.027
50.26	1.8139	≈12	Cu (200)	≈1.808
65.04	1.4329	32.1	α-Fe (200)	≈1.433
78.16	1.2219	20.3	Unassigned (see text)	—
82.36	1.1699	18.6	α-Fe (211)	≈1.170

A reflection at 78.16° (d = 1.2219 Å) could not be assigned with confidence. Its position is close to the reported spacing for a CsCl-type FeTi intermetallic, which would be a plausible interface reaction product, but the assignment rests on a single peak without corroborating reflections and is therefore not claimed here. Confirmation would require database-matched indexing and, ideally, complementary electron diffraction.

Notably, no clearly resolved TiC reflections were observed. Titanium carbide formation through reaction between transferred titanium and carbon liberated from the dielectric is a commonly reported hardening mechanism in EDC with Ti-bearing electrodes [4,5,11,12]. Its absence here, combined with the observation that hardness peaks at the lowest discharge energy, supports the interpretation advanced in Section 3.4: for this system the dominant strengthening contribution is grain refinement from rapid quenching rather than extensive in-situ carbide formation. Conditions favouring carbide formation would be expected to require the higher discharge energies that this study finds to yield lower hardness.

3.7. Confirmation experiment

Multi-response optimisation must reconcile conflicting factor preferences: thickness favours the highest current and pulse-on time, whereas hardness and roughness both favour the lowest. Because hardness and surface finish bear most directly on wear performance, and because both are optimised by the same settings, current level 1 was selected. The recommended optimum is therefore 4 A, 100 µs and 6 µs.

This combination coincides with Run 1 of the experimental array. A confirmation trial was performed at these settings and compared against the regression predictions (Fig. 8, Table 6).

Table 6. Confirmation experiment at the optimum condition (4 A, 100 µs, 6 µs).

Response	Predicted	Experimental	Deviation (%)
Coating thickness (µm)	16.20	15.80	2.47
Microhardness (HV0.2)	1050.0	1067.0	1.62
Surface roughness, Ra (µm)	2.45	2.30	6.12

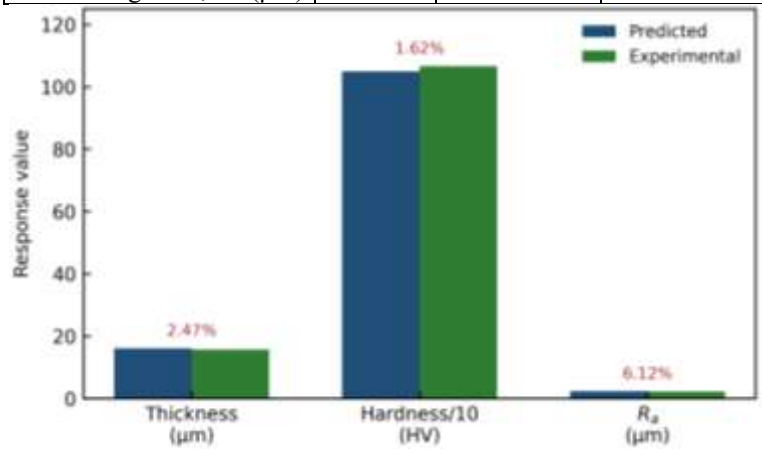

Fig. 8. Confirmation experiment: predicted against experimentally measured responses at the optimum condition, with percentage deviation indicated.

Agreement is close across all three responses, with deviations of 1.62% for hardness, 2.47% for thickness and 6.12% for roughness. That the hardness prediction is accurate to within 1.62% despite the weak linear model reflects the fact that the optimum lies at a factor level where the model and the data coincide closely. The confirmation result is the strongest available validation of the recommended parameter set.

3.8. Comparison with published work and limitations

The hardness achieved here compares favourably with reported EDC results. Devarani and Joshi [6] obtained approximately a fourfold hardness increase using a Ti–Al green compact on AISI P20 steel. Studies using Cr–Cu green compacts on AISI 4340 steel have reported values from 1008 HV to 1230.9 HV [14], comparable to the 1067.0 HV obtained here on a substantially softer and lower-cost substrate. Coating thicknesses of 15.8–48.9 µm fall within the range typical of green-compact EDC.

Three limitations should be stated. First, and most significantly, this study does not include scanning electron microscopy or energy-dispersive X-ray spectroscopy. Cross-sectional SEM would directly evidence the interface quality and coating continuity inferred here, and EDS would quantify the elemental composition that XRD establishes only qualitatively. The grain-refinement interpretation advanced in Section 3.4, while consistent with all available evidence, would be considerably strengthened by direct microstructural observation, and this is the primary avenue for further work.

Second, the single-replicate L9 design provides limited error degrees of freedom, which weakens the ANOVA F-tests, particularly for hardness. A replicated design would resolve whether the hardness effect reaches formal significance. Third, the study covers a single substrate grade, a single electrode composition ratio and a single dielectric, and long-term wear and corrosion performance were not assessed. Establishing whether the energy–hardness inversion persists across other Ti:Cu ratios and substrate grades would test the generality of the finding.

4. CONCLUSIONS

Electric discharge coating of AISI 1018 mild steel using an unsintered Ti–Cu (70:30 wt%) green-compact electrode was investigated through a Taguchi L9 design. The following conclusions are drawn.

(1) Coating microhardness reached 1067.0 HV0.2 against an untreated substrate baseline of 120–160 HV, an increase of approximately sevenfold, with coating thickness spanning 15.8–48.9 µm and surface roughness 2.30–7.60 µm across the parameter range examined.

(2) Discharge current is the dominant control factor for all three responses, contributing 62.3% of coating thickness variance, 57.8% of hardness variance and 88.7% of roughness variance. Pulse-on time is a significant secondary contributor to thickness only, and pulse-off time is minor throughout.

(3) Coating hardness does not increase with discharge energy. Peak hardness occurs at the lowest current and pulse-on time examined, attributed to the smaller and more rapidly quenched melt pool promoting grain-refinement strengthening rather than extensive reaction-phase formation.

(4) Because hardness and surface roughness are optimised by the same low-energy settings, no trade-off arises between surface hardness and surface finish for this system. Coating thickness alone requires opposing parameter selection.

(5) The optimum parameter combination of 4 A, 100 µs and 6 µs was validated by confirmation experiment with deviations of 1.62–6.12% between predicted and measured responses.
(6) X-ray diffraction confirmed crystalline α-Ti and Cu on the coated surface alongside α-Fe substrate reflections, establishing successful transfer of both electrode constituents. No clearly resolved TiC reflections were detected, consistent with grain refinement rather than carbide formation as the dominant strengthening mechanism under these conditions.

CRediT authorship contribution statement

Kishor H. Watane: Conceptualization, Methodology, Investigation, Formal analysis, Data curation, Writing – original draft, Visualization. Anoop D. Shirbhate: Conceptualization, Methodology, Supervision, Validation, Writing – review & editing, Project administration.

Declaration of competing interest

The authors declare that they have no known competing financial interests or personal relationships that could have appeared to influence the work reported in this paper.

Declaration of generative AI in the writing process

[To be completed by the authors in accordance with the journal's policy prior to submission.]

Data availability

Data will be made available on request.

ACKNOWLEDGEMENTS

The authors thank the Department of Production Engineering, Prof. Ram Meghe Institute of Technology & Research, Badnera, for providing laboratory facilities, and the technical staff who assisted with the coating experiments and characterisation.

REFERENCES

[1] Gangadhar A, Shunmugam MS, Philip PK. Surface modification in electro-discharge processing with a powder compact tool electrode. Wear 1991; 143:45–55.
[2] Mohri N, Saito N, Tsunekawa Y. Metal surface modification by electrical discharge machining with composite electrode. CIRP Ann 1993; 42:219–22.
[3] Simao J, Lee HG, Aspinwall DK, Dewes RC, Aspinwall EM. Workpiece surface modification using electrical discharge machining. Int J Mach Tools Manuf 2003; 43:121–8.
[4] Wang ZL, Fang Y, Wu PN, Zhao WS, Cheng K. Surface modification process by electrical discharge machining with a Ti powder green compact electrode. J Mater Process Technol 2002; 129:139–42.
[5] Furutani K, Saneto A, Takezawa H, Mohri N, Miyake H. Accretion of titanium carbide by electrical discharge machining with powder suspended in working fluid. Precis Eng 2001;25:138–44.
[6] Devarani N, Joshi SN. Electric discharge alloying of titanium and aluminium on AISI P20 mold steel. Surf Coat Technol 2020;397:125984.
[7] Krishna ME, Patowari PK. Parametric optimisation of electric discharge coating process with powder metallurgy tools using Taguchi analysis. Surf Eng 2013;29:703–11.
[8] Das A, Misra JP. Experimental investigation on surface modification of aluminum by electric discharge coating process using TiC/Cu green compact tool-electrode. Mach Sci Technol 2012;16:601–23.
[9] Chakraborty S, Kar S, Ghosh SK, Dey V. Parametric optimization of electric discharge coating on aluminium-6351 alloy with green compact silicon carbide and copper tool: a Taguchi coupled utility concept approach. Surf Interfaces 2017;7:47–57.
[10] Tijo D, Kumari S, Masanta M. Hard and wear resistant TiC-Fe composite coating produced by electrical discharge coating process. Silicon 2018;10:1625–37.
[11] Algodi SJ, Murray JW, Fay MW, Clare AT, Brown PD. Electrical discharge coating of nanostructured TiC-Fe cermets on 304 stainless steel. Surf Coat Technol 2016;307:639–49.
[12] Murray JW, Algodi SJ, Fay MW, Brown PD, Clare AT. Formation mechanism of electrical discharge TiC-Fe composite coatings. J Mater Process Technol 2017;243:143–51.
[13] Patel RK, Pradhan MK. Effect of different currents and compositions of Cu, MoS2 and hBN on the coating thickness of mild steel substrate using electric discharge coating. Mater Res Express 2022;9:056507.
[14] Oskueyan S, Hajialimohammadi A, Abedini V, et al. Statistical optimization of Cr–Cu green compact electrode parameters in the electrical discharge coating of AISI 4340 steel. Prog Addit Manuf 2026;11:2463–79.
[15] Elaiyarasan U, Satheeshkumar V, Senthilkumar C. Experimental analysis of electrical discharge coating characteristics of magnesium alloy using response surface methodology. Mater Res Express 2018;5:086501.
[16] Aspinwall DK, Dewes RC, Lee HG, Simao JMT. Electrical discharge surface alloying of Ti and Fe workpiece materials using refractory powder compact electrodes and Cu wire. CIRP Ann 2003;52:151–6.

[17] Kunieda M, Lauwers B, Rajurkar KP, Schumacher BM. Advancing EDM through fundamental insight into the process. CIRP Ann 2005;54:64–87.
[18] Ho KH, Newman ST. State of the art electrical discharge machining (EDM). Int J Mach Tools Manuf 2003;43:1287–300.
[19] Kruth JP, Stevens L, Froyen L, Lauwers B. Study of the white layer of a surface machined by die-sinking electro-discharge machining. CIRP Ann 1995;44:169–72.
[20] Van Dijck FS, Dutre WL. Heat conduction model for the calculation of the volume of molten metal in electric discharges. J Phys D Appl Phys 1974;7:899–910.
[21] Descoeudres A, Hollenstein C, Wälder G, Perez R. Time-resolved imaging and spatially resolved spectroscopy of electrical discharge machining plasma. J Phys D Appl Phys 2008;41:215207.
[22] Albinski K, Musiol K, Miernikiewicz A, Labuz S, Malota M. The plasma temperature in electrical discharge machining. Plasma Sources Sci Technol 1996;5:736–42.
[23] Hall EO. The deformation and ageing of mild steel: III discussion of results. Proc Phys Soc B 1951;64:747–53.
[24] Petch NJ. The cleavage strength of polycrystals. J Iron Steel Inst 1953;174:25–8.
[25] Dangwal S, Edalati K, Valiev RZ, Langdon TG. Breaks in the Hall–Petch relationship after severe plastic deformation of magnesium, aluminum, copper, and iron. Crystals 2023;13:413.
[26] Armstrong RW. The influence of polycrystal grain size on several mechanical properties of materials. Metall Trans 1970;1:1169–76.
[27] Akbarpour MR, Mirabad HM, Hemmati A, Kim HS. Processing and microstructure of Ti–Cu binary alloys: a comprehensive review. Prog Mater Sci 2022;127:100933.
[28] Xu Y, Jiang J, Yang Z, Zhao Q, Chen Y, Zhao Y. The effect of copper content on the mechanical and tribological properties of hypo-, hyper- and eutectoid Ti-Cu alloys. Materials 2020;13:3411.
[29] Taguchi G, Chowdhury S, Wu Y. Taguchi's quality engineering handbook. Hoboken: John Wiley & Sons; 2005.
[30] Ross PJ. Taguchi techniques for quality engineering. 2nd ed. New York: McGraw-Hill; 1996.
[31] Montgomery DC. Design and analysis of experiments. 8th ed. Hoboken: John Wiley & Sons; 2012.
[32] Cullity BD, Stock SR. Elements of X-ray diffraction. 3rd ed. Upper Saddle River: Prentice Hall; 2001.
[33] Monshi A, Foroughi MR, Monshi MR. Modified Scherrer equation to estimate more accurately nano-crystallite size using XRD. World J Nano Sci Eng 2012;2:154–60.
[34] Zhai W, Bai L, Zhou R, Fan X, Kang G, Liu Y, Zhou K. Recent progress on wear-resistant materials: designs, properties, and applications. Adv Sci 2021;8:2003739.
[35] Hutchings IM, Shipway P. Tribology: friction and wear of engineering materials. 2nd ed. Oxford: Elsevier; 2017.
[36] Krauss G. Steels: processing, structure, and performance. 2nd ed. Materials Park: ASM International; 2015.
[37] German RM. Powder metallurgy science. 2nd ed. Princeton: Metal Powder Industries Federation; 1994.
[38] ASTM E384-22. Standard test method for microindentation hardness of materials. West Conshohocken: ASTM International; 2022.
[39] ISO 4287:1997. Geometrical product specifications (GPS) — surface texture: profile method. Geneva: International Organization for Standardization; 1997.
[40] ASTM E3-11(2017). Standard guide for preparation of metallographic specimens. West Conshohocken: ASTM International; 2017.